Desalination and Water Treatment
www.deswater.com

doi: 10.1080/19443994.2015.1132475

57 (2016) 21685–21695
October

Taylor & Francis
Taylor & Francis Group

Performance improvement of membrane distillation of high-concentration saline solution with pulse feeding

Yuqin Xiong[a,b], Ting Peng[a,b], Zaifeng Shi[a,b,*], Qiang Lin[a,b], Meimei Zhang[a], Shichao Wang[a], Hao Li[a]

[a]*Key Laboratory of Water Pollution Treatment & Resource Reuse, Hainan Normal University, Haikou, Hainan 571158, P.R. China, Tel. +86 13036080306; email: 1240948944@qq.com (Y. Xiong), Tel. +86 15968660529; email: 18389946479@163.com (T. Peng), Tel. +86 13086013920; email: zaifengshi@163.com (Z. Shi), Tel. +86 13807654689; linqianggroup@163.com (Q. Lin), Tel. +86 15595694352, email: 2571921824@qq.com (M. Zhang), Tel. +86 18089877386, email: wangshichao207@qq.com (S. Wang), Tel. +86 18389371105; email: 782219860@qq.com (H. Li)*

[b]*College of Chemistry and Chemical Engineering, Hainan Normal University, Haikou, Hainan 571158, P.R. China*

Received 22 February 2015; Accepted 1 December 2015

ABSTRACT

In this study, digital time delay and solenoid valve were incorporated into sweeping gas membrane distillation to generate pulsatile feed. It can be found that shorter pulse length (0.5 s) at a smaller pulse frequency of 1 min^{-1} can most efficiently increase transmembrane flux, up to 16% improvement that of with steady flow. Moreover, $L16(4^5)$ orthogonal fractional factorial experiment results demonstrate that feed inlet temperature is the critical factor and the best combination of parameter values are feed flow rate of 50 L h^{-1}, feed inlet temperature of 333 K, coolant temperature of 283 K, gas-sweeping flow rate of 0.84 m^3 h^{-1}, and filling factor of 12.8%, separately. Lastly, pulsatile feed flow with saturated NaCl aqueous solution (333 K) not only delayed the occurrence of sharp flux decline due to membrane pore blocking caused by crystal deposition as compared to continuous flow, but enhanced the thermal efficiency by more than 56.7%. Observations of fouling status on the membrane surface show good agreement with the experimental results.

Keywords: Membrane distillation; Pulsatile feed; Crystal deposition; Fouling

1. Introduction

Membrane distillation (MD) is a promising thermally driven desalination technology for water treatment, with considerable permeability performance, high retention rate, and low or zero waste discharge under low operation temperature and pressure by only consuming readily accessible and inexpensive low-grade waste heat [1–6]. More significantly, the increasing salt concentration of the feed has a smaller effect on permeation flux than other conventional separation processes (e.g. reverse osmosis (RO)), whereby MD is well considered as a potential alternative desalination process for high-concentration salty water [7,8].

Nevertheless, mass transfer together with heat transfer in MD process is severely constrained by concentration and temperature polarization phenomenon [9–11]. Furthermore, when the salty concentration of feed is operated to the level of hypersaturation, salt

*Corresponding author.

1944-3994/1944-3986 © 2016 Balaban Desalination Publications. All rights reserved.

crystals deposition forming on the membrane results in pore blockage, introducing an additional resistance to the process of mass and heat transfer through membrane [12]. Hence, sharp transmembrane flux decrease is observed due to the thick surface fouling layer [13]. In order to overcome the obstacles of inadequate permeate flux and undesirable membrane scaling in the high-concentration MD applications, many efforts have been made to increase the shear force on the membrane walls, for instance, application of modified hollow fiber configurations with wavy geometries (twisted and braided) [14], placement of inducing components in the flow channel of membrane module (baffles, spacers, and turbulent promoter) [15–19], introduction of gas–liquid two-phase flow (gas bubbling) [20–27], the assistance of ultrasonic technique [28–30], and microwave irradiation [31–34]. Nevertheless, the above enhancement methods have some weaknesses, e.g. (1) properties of hydrophobic microporous membrane may easily be damaged by artificial distortion of membrane morphology; (2) hydraulic resistance is increased by assembly installed in the membrane module; (3) the energy consumption is increased by the introduction of gas and energy filed. Specially, feed is intermittently run controlled by digital time delay and solenoid valve [35], thereby creating pulsatile feed of better fluid dynamics in our research work. Furthermore, sweeping gas membrane distillation (SGMD) of periodic on and off rather than always running offers time-saving benefits for the same length of time. In spite of negligible increased energy consumption and equipment cost by digital time delay and solenoid, opening solenoid valve discontinuously can decrease the energy cost from a long-term point of view. To the best of our knowledge, the application of intermittent running method in SGMD process for desalination of high-concentration saline solution has not been reported to date.

2. Experimental

2.1. Feed preparation

The saturated NaCl solutions at the corresponding temperature of 303, 313, 323, and 333 K as feed stream were prepared by magnetically stirring of solid sodium chloride, supplied by Guangzhou Chemical Reagent Fac., China, in 1,000 ML of deionized water for 30 min.

2.2. Membrane module

Unlike PTFE and PP, polyvinylidene fluoride (PVDF) can be easily dissolved in common solvents such as n-Methyl-2-Pyrrolidone (NMP), dimethylacetamide (DMAC), and dimethylformamide (DMF). Meanwhile, it has a relatively low melting temperature of 443 K. Therefore, PVDF membranes can be fabricated either by NIPS, TIPS, or a combination of TIPS and NIPS process [36].

In this work, one commercially available PVDF hollow fiber MD membrane provided by Jack Co., China, is chosen to fabricate MD modules. The membrane modules are prepared with polypropylene (PC) housing. Parallel hollow fibers with packed density ranging from 12.8 to 32% were packed in a 230-mm-long module for flux assessment. The correlated characteristics of membrane and membrane module are presented in Table 1.

A laboratory scale of SGMD unit is employed and the experimental setup is shown schematically in Fig. 1. The salt feed solution was heated and maintained at the required temperature by a heater (constant temperature water bath), and then circulated to the shell side of a vertical up-flow module through a self-priming pump. Simultaneously, the coolant (the deionized water) is pumped into the condenser pipe by cooler (low-temperature cooling liquid circulating pump). The steam flowed through membrane pores into the lumen side of module and was swept by air pump into the condenser pipe to cool down. Then, the condensate was collected by permeate collector (conical flask) and was measured by balance. The temperature, pressure, and velocity of feed in both inlet and outlet of module were monitored by temperature indicator (TI), pressure indicator (PI), and rotameter, respectively. The conductivity of permeate is determined by a conductivity indicator (CI).

2.3. Membrane cleaning

Before SGMD experiments, the fresh membrane is cleaned chemically to remove irreversible fouling. Sequentially, acid cleaning is carried out with 0.5 wt.% citric acid solution for 30 min, and flushing by DI water is performed for 1 h at the feed flow rate of 80 L h^{-1} and at the feed inlet temperature of 333 K. The flux is held constant for SGMD test with tap water after regular flushing, indicating the adherent scale is removed completely. Instead, cleaning will be repeated.

2.4. MD process

Two types of SGMD with high-concentration NaCl solution are conducted, steady-flow membrane distillation (SSGMD) and pulsatile-flow membrane

Table 1
Characteristics of membrane and membrane module

Properties of PVDF hollow fiber membrane		Characteristics of membrane module	
Porosity ε (%)	78	Housing length (mm)	230
Contact angle (deg)	113 ± 1.7	Housing diameter, d_s[e] (mm)	20
Breaking strength (N)	3.07	No. of fibers, N	20–50
LEPw (bar)	4.038	Effective fiber length, L_{HF}[f] (mm)	180
Dimension (mm)	d_o[a]: 1.2 δ_m[b]: 0.15	Filling factor, FF (%)	12.8–32
Pore size (μm)	r_{max}[c]: 0.56 r_{mean}[d]: 0.22	Membrane area, A ($\times 10^{-2}$ m^2)	1.0174–2.5434

[a]d_o = outer diameter.
[b]δ_m = wall thickness.
[c]r_{max} = maximum pore size.
[d]r_{mean} = mean pore size.
[e]d_s = external surface diameter.
[f]L_{HF} = hollow fiber length.

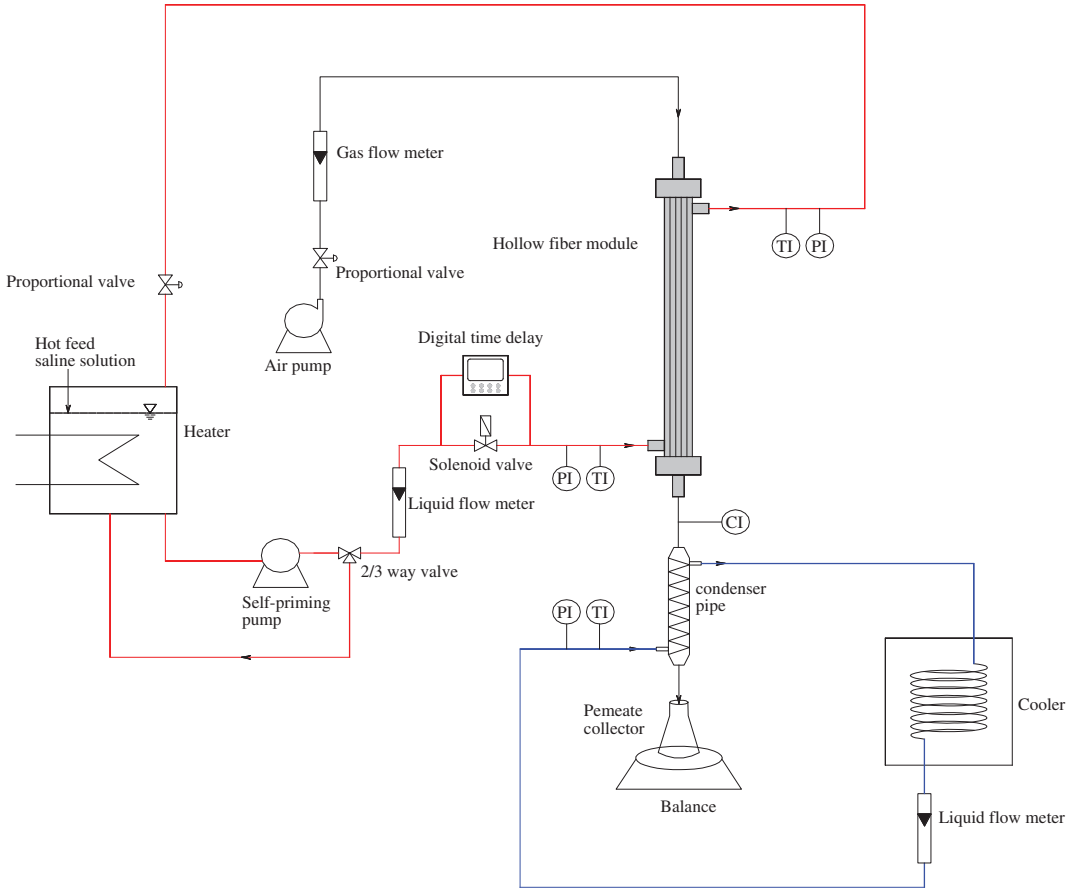

Fig. 1. Schematic diagram of SGMD system with pulsatile and steady feed flow.

distillation (PSGMD). Before each set of testing, the leakage check for modules was conducted by circulating DI water through the shell side for 10 min at ambient temperature. No sign of leakage is shown by no droplets emerging at the lumen side of membrane module. The whole experimental setup were

prerun for 30 min to confirm the permeate flux remaining in a stable state. The permeate flux is determined for every 5 min.

The influence of different pulse frequency (PF) and pulse length (PL) settings on transmembrane flux was investigated. A series of PSGMD experiments with saturated saline solution (323 K) are performed with various PLs (0.5, 1, 2, and 3 s) and different PFs (1, 1.5, 3, 6, and 12 min^{-1}), but the same feed flow rate (30 L h^{-1}), feed inlet temperature (323 K), coolant temperature (283 K), gas-sweeping velocity (0.64 m^3 h^{-1}), and filling factor (12.8).

In order to confirm the dominant factor(s) and optimize the PSGMD process, orthogonal fractional factorial (OFF) experiment [37,38] was designed by orthogonal design assistant software. As SGMD is both heart- and mass-transfer MSP, besides fill factor (FF) and coolant temperature can affect flow regime and cooling effect of water vapor. As such, feed flow rate (Q_f), feed inlet temperature ($T_{f\text{-}in}$) on the shell side, gas-sweeping flow rate (Q_a) on the lumen side, FF, and coolant temperature (T_c) are the main operating parameters influencing the transmembrane flux. Hence, in this study, OFF experimental layout is made with five factors under four levels by the optimal pulse parameters as shown in Table 2. Table 3 shows the details of $L16(4^5)$ orthogonal array, where L refers to orthogonal layout; 16 is the number of experimental runs; 4 is the level number of each researched factor, and 5 is the researched factors number. Each row numbered from 1 to 16 in Table 3 indicates a run at specified level for respective factor.

For 300-min pulse case and non-pulse case with the optimum combination, the fluxes and pictures of crystal forming on the membrane obtained by scanning electron microscopy (SEM) were studied. After the two circulated experiment runs, the PVDF hollow fiber membranes were extracted from the membrane modules carefully and put into a heating oven for fan-drying to a constant weight at 303 K. Before the commencement of photograph, the membrane samples of 10-mm length were coated with a thin gold layer. The voltage was 5.0 kV and magnification was 40×.

3. Result and discussion

3.1. Influence of PF–PL setting

The effect of PF–PL set was investigated at a low Q_f of 30 L h^{-1}, as it would be difficult to study the influence of pulse feeding on flux at higher Q_f. Four PLs, 0.5, 1, 2, 3 s, were investigated at five PFs: every 5 s, each 10 s, once each 20 s, once every 40 s, once per minute for 60-min experiment operation. The results are shown in Fig. 2.

Compared with the non-pulse case, the results show that the flux for pulse case increases to some extent. This enhancement may be due to the fiber movement and enhanced mixing caused by water hammer [39] with intermittent running. With the flow disturbance, the thermal boundary layer in the feed side may be reduced, leading to an increase in the transmembrane temperature difference (driving force). As a result, the permeation rate increases somewhat.

In addition, it is observed that a higher transmembrane flux was possible with the smaller PF and shorter PL. The optimum PF–PL setting is 1 min^{-1} to 0.5 s, and the flux is up to 2.065 L m^{-2} h^{-1}. When PF is constant, the transmembrane flux (PL = 0.5 s) is much higher than that with PL = 1, 2, 3 s. At the identical PL, the transmembrane flux increases gradually with the decrease in PF. This tendency illustrates that water hammer tends to be more effective in the shorter PL and smaller PF. This may be because the permeate flux is dominated by the effective MD time rather than water hammer, which can evoke the fiber movement and secondary flows and effectively disrupts the boundary layer and promotes local mixing near the membrane surface. Nevertheless, the permeation flux (PF = 12 min^{-1}, PL = 1, 2, 3 s) is lower than that of non-pulse case. With the increase in PL, the

Table 2
The factors and levels of the OFF experiment

Factor		Units	Level			
			1	2	3	4
A	Feed flow rate, Q_f	L h^{-1}	20	30	40	50
B	Feed inlet temperature, $T_{f\text{-}in}$	K	303	313	323	333
C	Coolant temperature, T_c	K	283	288	293	298
D	Gas-sweeping flow rate, Q_a	m^3 h^{-1}	0.54	0.64	0.74	0.84
E	Filling Factor, FF	%	12.8	19.2	25.6	32

Table 3
Operating conditions of each experiment based on $L16(4^5)$ orthogonal array

Run no.	Factors					
	Q_f (L h^{-1})	$T_{f\text{-}in}$ (K)	T_c (K)	Q_a (m^3 h^{-1})	FF (%)	J_p (L m^{-2} h^{-1})
1	20	30	10	0.54	12.8	0.965
2	20	40	15	0.64	19.2	0.913
3	20	50	20	0.74	25.6	1.141
4	20	60	25	0.84	32	1.301
5	30	30	15	0.74	32	0.440
6	30	40	10	0.84	25.6	1.038
7	30	50	25	0.54	19.2	0.898
8	30	60	20	0.64	12.8	2.423
9	40	30	20	0.84	19.2	0.664
10	40	40	25	0.74	12.8	0.917
11	40	50	10	0.64	32	1.517
12	40	60	15	0.54	25.6	1.929
13	50	30	25	0.64	25.6	0.088
14	50	40	20	0.54	32	0.522
15	50	50	15	0.84	12.8	2.460
16	50	60	10	0.74	19.2	2.541
I_1	4.320	2.157	6.061	4.314	6.765	
I_2	4.799	3.390	5.742	4.941	5.016	
I_3	5.027	6.016	4.750	5.039	4.196	
I_4	5.611	8.194	3.204	5.463	3.780	
$\bar{I}_1$	1.080	0.539	1.515	1.079	1.691	Y = 1.235
$\bar{I}_2$	1.200	0.848	1.436	1.235	1.254	
$\bar{I}_3$	1.257	1.504	1.188	1.260	1.049	
$\bar{I}_4$	1.403	2.049	0.801	1.366	0.945	

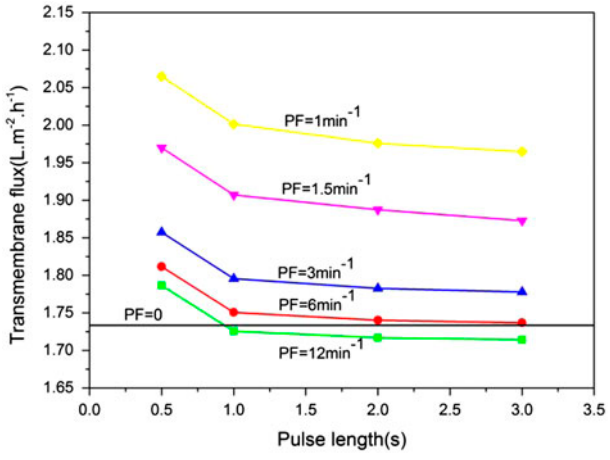

Fig. 2. Effect of PF–PL combination on transmembrane flux for 60-min PSGMD experiments. (saturated NaCl solution as feed: Q_f = 30 L h^{-1}, $T_{f\text{-}in}$ = 323 K, T_c = 283 K, Q_a = 0.74 m^3 h^{-1} and FF = 12.8%).

feed is separated from the membrane surface, and the MD process is halted and water hammer seems to be useless, resulting inthe decrease of permeate flux.

3.2. Result and analysis of OFF experiments

3.2.1. Control factors to transmembrane flux

As outlined in Table 2, the feed flow rate, feed inlet temperature, coolant temperature, gas-sweeping flow rate, and filling factor were selected as the control factor for the OFF experimental design to assess the PSGMD performance with PF/PL = 1 min^{-1}/0.5 s. The pure water transmembrane flux was chosen as the quality characteristics in the $L16(4^5)$ orthogonal array design. The sixteen experiments were all carried out for 1 h according to the experiment design arrangement summarized in Table 3.

The average pure water production flux (L m^{-2} h^{-1}) for the sixteen experiments can be determined by Eq. (1) from the data in Table 3:

$$Y = \frac{1}{16}\Sigma y_n \quad (n = 1, 2, 3, \ldots, 16) \tag{1}$$

where y_n is the transmembrane flux of the nth experiment run in the OFF test. I_1, I_2, I_3, I_4 are the total transmembrane flux of specific factor at each level. The influence of each factor on the PSGMD

performance can be assessed by the average permeation flux for each level ($\bar{I}_1$, $\bar{I}_2$, $\bar{I}_3$, $\bar{I}_4$) in graphical form shown in Fig. 3.

Fig. 3(a) shows the main effect of feed flow rate (20, 30, 40, 50 L h^{-1}) on the distillate flux. As can be observed, with an increase in Q_f from 20 to 50 L h^{-1}, the permeate flux increases from ~1.080 to ~1.403 L m^{-2} h^{-1}. The initial increase in Q_f increased Reynolds number (*Re*) and thereby improves the hydrodynamics adjacent to the membrane. Consequently, the thickness of the thermal and solute boundary layers near the membrane is decreased; thereby, temperature and concentration polarization effect is weakened. The increase in distillate flux from 20 to 50 L h^{-1} could be supported by this hypothesis.

The second studied factor is $T_{f\text{-}in}$, and four levels for $T_{f\text{-}in}$ (303, 313, 323, and 333 K) were tested. As can be seen from Fig. 3(b), an increase in the feed temperature

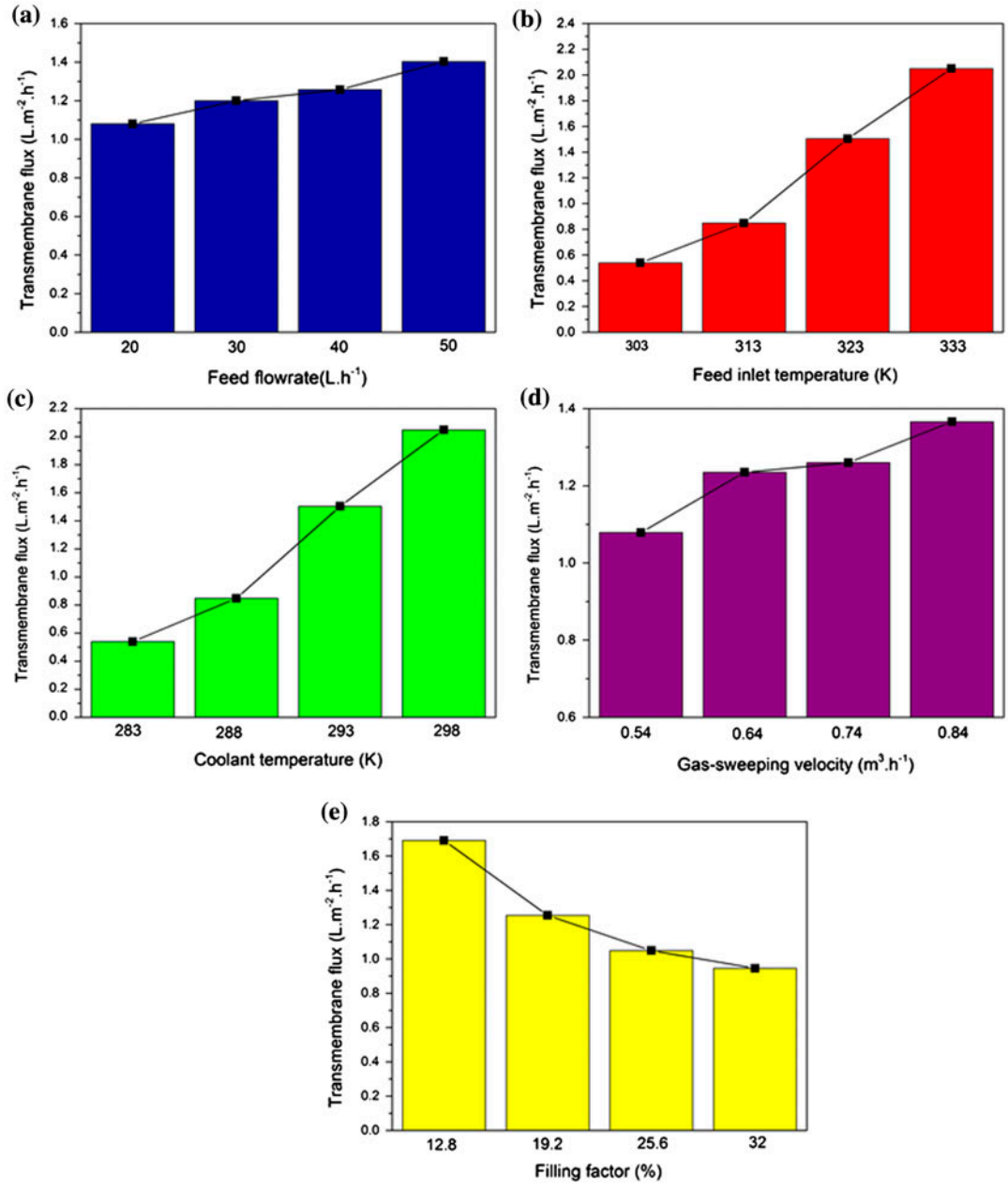

Fig. 3. Factor effect chart on transmembrane flux with pulsatile flow (PF/PL = 1 min^{-1}/0.5 s, running time of each OFF experiments = 1 h): (a) Q_f, (b) $T_{f\text{-}in}$, (c) T_c, (d) Q_a, and (e) FF.

leads to an increase in the distillate flux, which agrees well with those obtained in literature [40]. This is due to the fact that the nature of the MD process is thermal-driven separation technology and the vapor pressure is related exponentially to the temperature of feed, so higher transmembrane flux can be obtained.

Fig. 3(c) shows a graph of the permeation flux as a function of T_c in the PSGMD process. The permeation flux shows a monotonic decrease with increasing coolant temperature. That is because increasing T_c reduces the transmembrane temperature difference, thus the vapor pressure driving force for penetration through the membrane is declined, inducing a decrease in the water permeation flux [41].

In the PSGMD process, the distillate side consists of a sweeping gas (dried and filtered air) which sweeps the evaporated vapor molecules. Therefore, the effect of variation of Q_a was investigated. Fig. 3(d) shows that the increase in Q_a basically leads to the increase in the flux value from 1.079 to 1.366 L m^{-2} h^{-1} [42,43]. An increase in the sweeping gas velocity in a constant channel depth could increase the turbulence effect in the permeate side. This leads to vapor pressure reduction in the cold side (permeate side), which consequently leads to an increase in the vapor pressure gradient.

The final explored factor was FF in different module configurations; Fig. 3(e) shows the transmembrane flux as a function of FF. The experimental results reveal that the transmembrane flux decreases with increasing FF. That probably due to *Re* of feed flow in a loosely FF module is higher than that of a tightly packed configuration under the same Q_f. This result indicates that membrane module with higher FF has more passive effect on flux, i.e. driving force decreases with increasing FF in a MD module.

In summary, the OFF design experiments indicate the PSGMD process should run at a relatively high Q_f, $T_{f\text{-}in}$, and Q_a while relatively low in T_c and FF.

3.2.2. Range analysis and analysis of variance

Range analysis is used to identify the principal operating parameters and to determine optimal operating conditions for the results of OFF design experiments. The difference between the average permeation flux for the four levels of the kth (i.e. k = 1–4) and the average permeation for the 16 runs (D_t) can be determined by the given equation:

$$D_t = \bar{I}_t - Y \quad (t = A, B, C, D) \tag{2}$$

There are four values of D_t, for each of the five factors. For each factor, there will be maximum and minimum values of D_t denoted by R_{max} and R_{min}, respectively.

The metric T defined by Eq. (3) is a measure of the importance of the particular factor in terms of its influence on the permeation flux:

$$T = R_{max} - R_{min} \tag{3}$$

A large value of T implies that varying the particular factor causes a large change in the permeation flux.

D_{tk} is defined to be the value of D for the tth factor at the kth level. The optimal values of the factor can be estimated from the largest values of D_{tk}. Table 4 summarizes the resulting values of D_1, D_2, D_3, D_4, R_{max}, R_{min}, and T for the five factors, namely Q_f, $T_{f\text{-}in}$, T_c, Q_a, and FF in the range analysis. It can be seen that $T_{f\text{-}in}$ is the principal factor influencing the performance of the PSGMD process for the largest T value (1.510). The inspection of the D_{tk} values in Table 4 indicates the following: $D_{A4} > D_{A3} > D_{A2} > D_{A1}$; $D_{B4} > D_{B3} > D_{B2} > D_{B1}$; $D_{C1} > D_{C2} > D_{C3} > D_{C4}$; $D_{D4} > D_{D3} > D_{D2} > D_{D1}$; $D_{E1} > D_{E2} > D_{E3} > D_{E4}$. This implies that the optimal values of the four factors based on 16 runs for OFF experiment design are the following: Q_f = 50 L h^{-1}; $T_{f\text{-}in}$ = 333 K; T_c = 283 K; Q_g = 0.84 m^3 h^{-1}; FF = 12.8%. However, it should be pointed out that these values do not represent a global optimum but rather optimum values based on OFF experiment.

The analysis of variance (ANOVA) is applied to investigate which PSGMD operating variable significantly affects the performance characteristics. This is accomplished by separating the total variability of each level, which is measured by the sum of the

Table 4
Range analysis

No. of factor	D_1	D_2	D_3	D_4	R_{max}	R_{min}	T
A	−0.155	−0.035	0.022	0.168	0.168	−0.155	0.323
B	−0.696	−0.387	0.269	0.814	0.814	−0.696	1.510
C	0.280	0.201	−0.047	−0.434	0.280	−0.434	0.714
D	−0.156	0.000	0.025	0.131	0.131	−0.156	0.287
E	0.456	0.019	−0.186	−0.290	0.456	−0.290	0.746

Table 5
Results of the ANOVA

Factor	DOF	Sum of squares	Variances	Percent (%)
Q_f	3	0.216	0.108	2.57
$T_{f\text{-}in}$	3	5.473	2.737	65.15
T_c	3	1.237	0.619	14.73
Q_g	3	0.169	0.085	2.01
FF	3	1.309	0.655	15.58
Error	–	–	–	0.01%
Total	15	8.400		100.00

squared deviations from the total mean of the responses, into contribution by each PSGMD operating variable operating variables in the total sum of the squared deviations could be used to and the error. The contribution percentage by each of the operating variables can be used to evaluate the importance of the factor change on the performance characteristics.

Results of ANOVA are shown in Table 5 indicating that $T_{f\text{-}in}$ is the most effective factor in the PSGMD process for high-concentration saline solution for its highest contribution (65.15%). Moreover, the contribution of errors was only 0.01% which is in the reasonable range.

3.3. Comparison of PSGMD and SSGMD experiments

3.3.1. Transmembrane flux

Fig. 4. shows the comparison of the transmembrane flux vs. time with two different flow configurations, pulsatile flow (PF/PL = 1 min^{-1}/0.5 s) and steady flow. saturated NaCl solution (333 K) as feed, the optimum operating parameters gained from OFF experiment were kept constant, : Q_f = 50 L h^{-1}; $T_{f\text{-}in}$ = 333 K; T_c = 283 K; Q_g = 0.84 m^3 h; FF = 12.8%. Comparative experiments between SSGMD and PSGMD are both run for 300 min.

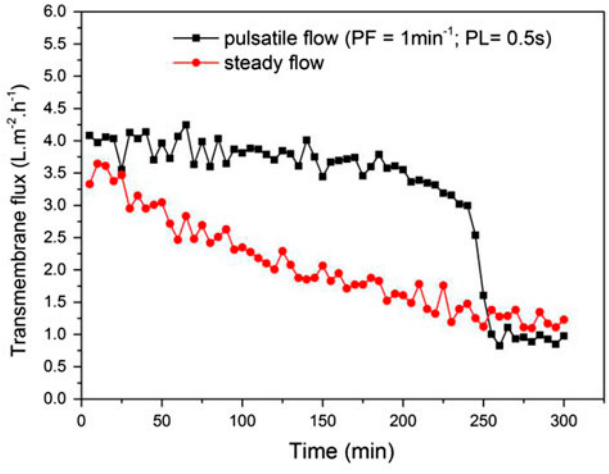

Fig. 4. Transmembrane flux vs. time with pulsatile flow (PF/PL = 1 min^{-1}/0.5 s) and continuous flow (saturated NaCl solution (333 K)) as feed: Q_f = 50 L h^{-1}, $T_{f\text{-}in}$ = 333 K, T_c = 283 K, Q_a = 0.84 m^3 h^{-1} and FF = 12.8%).

As can be seen, the transmembrane flux with pulsatile flow is significantly larger than that with steady flow during 0–250 min. For steady flow, it is apt to form temperature polarization phenomena easily at the laminar conditions due to a thick temperature layer; while for pulsatile flow, water hammer phenomenon can introduce a turbulence flow and increase transmembrane driving force with a reduced temperature boundary layer. The transmembrane flux varies with time according to downward-sloping curve for steady flow and inverse "S" shape for pulsatile flow; this is the most important difference between the pulsatile flow and steady flow.

For steady flow, the transmembrane flux is inversely proportional to time on account of membrane pores pocked by crystal packing over time. For pulsatile flow, it is clearly seen that the variation of flux with time can be divided into three states: sub-steady (0–200 min), pre-steady (200–250 min), and steady state (250 min). In sub-steady state, flux drops slightly with time. After reaching pre-steady state, the flux begins to decline significantly for 50 min until it reaches the steady state with insignificant pure water production. The concentration of saturated NaCl solution is ~27.16% on the membrane surface; therefore, the solution of the boundary layer differs greatly from the bulk solution such that the temperature polarization resistance and membrane fouling resistance increase sharply, resulting in sharp decrease of transmembrane flux. However, the pulsatile flow can induce the fiber vibration and promote the mixture of internal feed, leading to the decrease in thermal boundary layer and increase in driving force. Therefore, the flux can maintain a higher level and the crystals are harder to be formed on the membrane surface. But, with the increased time, more and more crystals are formed in the feed solution for pulsatile flow, water hammer cannot prevent crystal deposition on the membrane surface anymore, so the transmembrane flux declined dramatically (t = 200 min). From 250 to 300 min, the transmembrane flux keep steady state at the lower level (~1.1 L m^{-2} h^{-1} for steady flow and ~1.0 L m^{-2} h^{-1} for pulsatile flow), resulting from most of the membrane pores blocked by NaCl crystals.

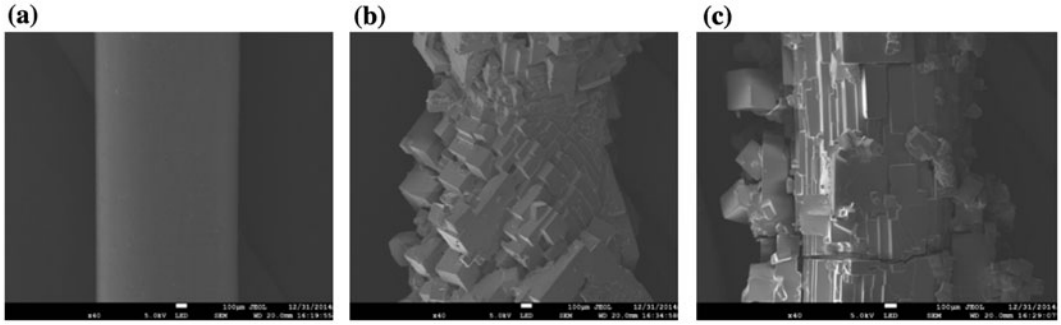

Fig. 5. (a) SEM image of unfouled membrane surface, (b) SEM image of membrane surface after 300-min SSGMD, and (c) SEM image of membrane surface after 300-min PSGMD (PF/PL = 1 min^{-1}/0.5 s).

3.3.2. NaCl crystal morphology on membrane surface

To associate the flux decline phenomenon with the tendency of scaling formation on the membrane surface, Fig. 5 shows the SEM pictures of the surfaces of three membrane systems: fresh membrane, fouled membrane with steady flow, and fouled membrane with pulsatile flow.

In Fig. 5(a), no crystal deposition is observed from the fresh membrane surface. After 300-min operation, complete crystal coverage on the membrane surface is observed in Fig. 5(b) and (c) in agreement with flux results presented in Fig. 4. NaCl crystals deposited on the membrane surface for SSGMD process is thick and dense; while the thinner crystals with gaps deposition is adherent to the membrane surface for PSGMD process. Taking the pulsatile flow as a example, water hammer induced by valve on and off can lead to hydraulic and membrane vibration and excessive oscillations, so crystals adjacent to the membrane surface may be destroyed and detached. It can be concluded that the SSGMD process is vulnerable to severe salt deposition, while PSGMD process can help enhance the SGMD performance with a higher permeation flux and delay the critical point for major flux decline. More importantly, it can illustrate that the PSGMD process is available for such high-concentration feed solution.

3.3.3. Thermal efficiency

For SGMD process, the values of thermal efficiency were obtained from the ratio of the part of the heat which contributes to evaporation to the total heat input in the module. It was found that thermal efficiency increases from 24.81 for steady flow to 38.88% for pulsatile flow (PF/PL = 1 min^{-1}/0.5 s), i.e. an increase in thermal efficiency of 56.7%. In order to reduce energy consumption, low-grade and/or alternative energy sources such as solar (either thermal or PV) energy or waste heats are available [44].

4. Conclusion

It has been shown that permeation flux can be increased during PSGMD process of high-concentration of saline solution by pulse feeding. Among PF/PL combination investigated, it was found that PF/PL of 1 min^{-1}/0.5 s was optimal and the transmembrane flux is up to 2.065 L m^{-2} h^{-1}, 19.13% increase relative to steady flow.

The PSGMD process has been introduced for the desalinating of the high-concentration NaCl solution. The effect of various operating variables on transmembrane flux has been investigated. The distillate flux enhancement increases with the increase of Q_f, $T_{f\text{-}in}$, and Q_a and with the decrease of T_c and FF. Based on the range analysis and ANOVA, the best experimental conditions are Q_f = 50 L h^{-1}; $T_{f\text{-}in}$ = 333 K; T_c = 283 K; Q_a = 0.84 m^3 h^{-1}; FF = 12.8% and the distillate flux is dominated by $T_{f\text{-}in}$.

When membrane pores are blocked, the PSGMD process can postpone flux sharp decrease effectively, prior to that of SSGMD process. As for the dramatically declined flux, back flushing may be a potential strategy to peel off the crystals from the surface of membrane to reduce this decay or extend the operation time. Pulse feeding cooperated with back flushing to improve the membrane performance for high-concentration saline of MD process will be discussed in future research.

It can be seen that thermal efficiency for PSGMD process is reduced to 24.81, 56.7% improvement than that of SSGMD process. Furthermore, the availability of the low-cost energy (e.g. solar energy) can be considered to be used for the PSGMD process.

Acknowledgment

Financial supports from the Department of Science & Technology of Hainan Province, P.R. China for program fund (XH201421) and of Hainan provincial College Students' Innovation and Entrepreneurship Training Program (20140058) are greatly acknowledged.

References

[1] S. Kubota, K. Ohta, I. Hayano, M. Hirai, K. Kikuchi, Experiments on seawater desalination by membrane distillation, Desalination 69 (1988) 19–26.
[2] F. Banat, R. Jumah, M. Garaibeh, Exploitation of solar energy collected by solar stills for desalination by membrane distillation, Renewable Energy 25 (2002) 293–305.
[3] R.A. Tufa, E. Curcio, E. Brauns, W. van Baak, E. Fontananova, G.D. Profio, Membrane distillation and Reverse Electrodialysis for Near-zero liquid discharge and low energy seawater desalination, J. Membr. Sci. 496 (2015) 325–333.
[4] K.W. Lawson, D.R. Lloyd, Membrane distillation, J. Membr. Sci. 124 (1997) 1–25.
[5] K.W. Lawson, D.R. Lloyd, Membrane distillation. I. Module design and performance evaluation using vacuum membrane distillation, J. Membr. Sci. 120 (1996) 111–121.
[6] A.M. Alklaibi, N. Lior, Membrane-distillation desalination: Status and potential, Desalination 171 (2005) 111–131.
[7] M.T. Chan, A.G. Fane, J.T. Matheickal, R. Sheikholeslami, Membrane distillation crystallization of concentrated salts—Flux and crystal formation, J. Membr. Sci. 257 (2005) 144–155.
[8] X.S. Ji, E. Curcio, S.A. Obaidani, G.D. Profio, E. Fontananova, Membrane distillation-crystallization of seawater reverse osmosis brines, Sep. Purif. Technol. 71 (2010) 76–82.
[9] L.M. ínez-Díez, M.I. Vázquez-González, Temperature and concentration´polarization in membrane distillation of aqueous salt solutions, J. Membr. Sci. 156 (1999) 265–273.
[10] V. Calabro, E. Drioli, Polarization phenomena in integrated reverse osmosis and membrane distillation for seawater desalination and waste water treatment, Desalination 108 (1997) 81–82.
[11] R.W. Schofield, A.G. Fane, C.J.D. Fell, R. Macoun, Factors affecting flux in membrane distillation, Desalination 77 (1990) 279–294.
[12] R.W. Schofield, A.G. Fane, C.J.D. Fell, Heat and mass transfer in membrane distillation, J. Membr. Sci. 33 (1987) 299–313.
[13] L.D. Tijing, Y.C. Woo, J.S. Choi, S. Lee, S.H. Kim, H.Y. Shon, Fouling and its control in membrane distillation —A review, J. Membr. Sci. 475 (2015) 215–244.
[14] M.M. Teoh, S. Bonyadi, T.S. Chung, Investigation of different hollow fiber module designs for flux enhancement in the membrane distillation process, J. Membr. Sci. 311 (2008) 371–379.
[15] N. Al-Bastaki, A. Abbas, Use of fluid instabilities to enhance membrane performance: A review, Desalination 136 (2001) 255–262.
[16] M.N. Chernyshov, G.W. Meindersma, Comparison of spacers for temperature polarization reduction in air gap membrane distillation, Desalination 183 (2005) 363–374.
[17] J. Phattaranawik, R. Jiraratananon, A.G. Fane, Mass flux enhancement using spacer filled channels in direct contact membrane distillation, J. Membr. Sci. 187 (2001) 193–201.
[18] M. Shakaib, S.M.F. Hasani, I. Ahmed, R.M. Yunus, A CFD study on the effect of spacer orientation on temperature polarization in membrane distillation modules, J. Membr. Sci. 284 (2012) 332–340.
[19] A. Tamburini, P. Pitò, A. Cipollina, G. Micale, M. Ciofalo, A thermochromic liquid crystals image analysis technique to investigate temperature polarization in spacer-filled channels for membrane distillation, J. Membr. Sci. 447 (2013) 260–273.
[20] Y. Lu, Z. Ding, L. Liu, Z. Wang, R. Ma, The influence of bubble characteristics on the performance of submerged hollow fiber membrane module used in microfiltration, Sep. Purif. Technol. 61 (2008) 89–95.
[21] T.M. Qaisrani, W.M. Samhaber, Impact of gas bubbling and backflushing on fouling control and membrane cleaning, Desalination 266 (2011) 154–161.
[22] Z. Ding, L. Liu, Z. Liu, R. Ma, The use of intermittent gas bubbling to control membrane fouling in concentrating TCM extract by membrane distillation, J. Membr. Sci. 372 (2011) 172–181.
[23] G. Chen, X. Yang, R. Wang, Performance enhancement and scaling control with gas bubbling in direct contact membrane distillation, Desalination 308 (2013) 47–55.
[24] G. Chen, X. Yang, Y. Lu, R. Wang, A.G. Fane, Heat transfer intensification and scaling mitigation in bubbling-enhanced membrane distillation for brine concentration, J. Membr. Sci. 470 (2014) 60–69.
[25] Y. Wibisono, E.R. Cornelissen, A.J.B. Kemperman, W.G.J. van der Meer, K. Nijmeijer, Two-phase flow in membrane processes: A technology with a future, J. Membr. Sci. 453 (2014) 566–602.
[26] G. Chen, X. Yang, Y.H. Lu, R. Wang, A.G. Fane, Heat transfer intensification and scaling mitigation in bubbling-enhanced membrane distillation for brine concentration, J. Membr. Sci. 470 (2014) 60–69.
[27] C.R. Wu, Z.G. Li, J.H. Zhang, Y. Jia, Q.J. Gao, X.L. Lu, Study on the heat and mass transfer in air-bubbling enhanced vacuum membrane distillation, Desalination 373 (2015) 16–26.
[28] C. Zhu, G.L. Liu, Modeling of ultrasonic enhancement on membrane distillation, J. Membr. Sci. 176 (2000) 31–41.
[29] D.Y. Hou, G.H. Dai, H. Fan, H.J. Huang, J. Wang, An ultrasonic assisted direct contact membrane distillation hybrid process for desalination, J. Membr. Sci. 476 (2015) 59–67.
[30] D.Y. Hou, Z.X. Wang, G.L. Li, H. Fan, J. Wang, H.J. Huang, Ultrasonic assisted direct contact membrane distillation hybrid process for membrane scaling mitigation, Desalination 375 (2015) 33–39.
[31] Z.G. Ji, J. Wang, Effect of microwave irradiation on vacuum membrane distillation, J. Membr. Sci. 429 (2013) 473–479.
[32] Z.G. Ji, J. Wang, Effect of microwave irradiation on typical inorganic salts crystallization in membrane distillation process, J. Membr. Sci. 455 (2014) 24–30.

[33] D. Qu, Z.M. Qiang, S.H. Xiao, Q.X. Liu, Y.Q. Lei, T.T. Zhou, Degradation of reactive black 5 in a submerged photocatalytic membrane distillation reactor with microwave eletrodeless lamps as light source, Sep. Purif. Technol. 122 (2014) 54–59.
[34] K. Werth, P. Lutze, A.A. Kiss, A.I. Stankiewicz, G.D. Stefanidis, A. Górak, A systematic investigation of microwave-assisted reactive distillation: Influence of microwaves on separation and reaction, Chem. Eng. Process. Process Intensif. 93 (2015) 87–97.
[35] C. Wilharm, V.G.J. Rodgers, Significance of duration and amplitude in transmembrane pressure pulsed ultrafiltration of binary protein mixtures, J. Membr. Sci. 121 (1996) 217–228.
[36] P. Wang, T.S. Chung, Recent advances in membrane distillation processes: Membrane development, configuration design and application exploring, J. Membr. Sci. 474 (2015) 39–56.
[37] M.T. Ravanchi, T. Kaghazchi, A. Kargari, M. Soleimani, A novel separation process for olefin gas purification: Effect of operating parameters on separation performance and process optimization, J. Taiwan Inst. Chem. Eng. 40 (2009) 511–517.
[38] G. Chen, Y.H. Lu, W.B. Krantz, R. Wang, A.G. Fane, Optimization of operating conditions for a continuous membrane distillation crystallization process with zero salty water discharge, J. Membr. Sci. 450 (2014) 1–11.
[39] A. Bergant, A.R. Simpson, Water hammer with column separation: A historical review, J. Fluids Struct. 22 (2006) 135–171.
[40] M.M.A. Shirazi, A. Kargari, M. Tabatabaei, Evaluation of commercial PTFE membranes in desalination by direct contact membrane distillation, Chem. Eng. Process. Process Intensif. 76 (2014) 16–25.
[41] H. Yu, X. Yang, R. Wang, A.G. Fane, Numerical simulation of heat and mass transfer in direct membrane distillation in a hollow fiber module with laminar flow, J. Membr. Sci. 384 (2011) 107–116.
[42] C. Cojocaru, M. Khayet, Sweeping gas membrane distillation of sucrose aqueous solutions: Response surface modeling and optimization, Sep. Purif. Technol. 81 (2011) 12–24.
[43] M. Khayet, C. Cojocaru, A. Baroudi, Modeling and optimization of sweeping gas membrane distillation, Desalination 287 (2012) 159–166.
[44] S.E. Hosseini, A.M. Andwari, M.A. Wahid, G. Bagheri, A review on green energy potentials in Iran, Renewable Sustainable Energy Rev. 27 (2013) 533–545.